A CONTINUOUS ADJOINT FORMULATION WITH EMPHASIS TO AERODYNAMIC–TURBOMACHINERY OPTIMIZATION

Dimitrios I. Papadimitriou[*] and Kyriakos C. Giannakoglou[†]

[*]National Technical University of Athens, Lab. of Thermal Turbomachines
P.O. Box 64069, 15710, Athens, Greece
e-mail: dpapadim@mail.ntua.gr
web page: http://velos0.ltt.mech.ntua.gr/research/
[†] National Technical University of Athens, Lab. of Thermal Turbomachines
P.O. Box 64069, 15710, Athens, Greece
e-mail: kgianna@central.ntua.gr

Key words: Continuous Adjoint, Inverse Design, Optimization, Losses Minimization, Turbomachines

Abstract. *This paper summarizes progress, recently made in the Lab. of Thermal Turbomachines of NTUA, on the formulation and use of the continuous adjoint methods in aerodynamic shape optimization problems. The basic features of state of the art adjoint methods and tools which are capable of handling arbitrary objective functions, cast in the form of either boundary or field integrals, are presented. Starting point of the presentation is the formulation of the continuous adjoint method for arbitrary integral objective functionals in problems governed by arbitrary, linear or nonlinear, first or second order state pde's; the scope of this section is to demonstrate that the proposed formulation is general without being restricted to aerodynamics. It is noticeable that, regardless of the type of functional (field of boundary integral) the expressions of its gradient with respect to the design variables include boundary integrals only. Thus, the derived adjoints can be used with either structured or unstructured grids and there is no need for repetitive remeshing or computation of field integrals which increase the CPU cost and deteriorate the computational accuracy. Then, the presentation focuses on aerodynamic shape optimization problems governed by the compressible fluid flow equations, numerically solved through a time-marching formulation and an upwind discretization scheme for the convection terms. Two design problems, namely the inverse design of a 2D cascade at inviscid flow conditions (used as a test bed for the assessment of three descent algorithms based on the same gradient information) and the design optimization of a 3D peripheral compressor cascade for minimum viscous losses are presented. For the latter, the flow is turbulent and the field integral of entropy generation, recently proposed by the same authors, is used as objective function.*

1

1 INTRODUCTION

Historically, Lions[1] was the first to handle, using control theory, a design problem governed by pde's. Later, Pironneau[2] introduced the adjoint method in design problems governed by elliptic equations and Jameson[3] extended it to transonic flows. Nowadays, the relevant literature is large; it includes applications such as inverse design of airfoils and wings,[4,5] sonic boom reduction[6,7] supersonic design,[8,9] shock minimization[10,11] and turbomachinery designs for steady or unsteady flows.[12–14]

The so–called continuous adjoint method, where this paper focuses on, relies on a mathematical development which considers the variation in the augmented objective function F_{aug}; the latter is formed by the flow equations R multiplied by the Lagrange multipliers (Ψ, the so–called adjoint or co–state variables) and added to the objective function F. By eliminating the effect of variations in flow quantities on the variation in F_{aug}, the adjoint equations and their boundary conditions are derived. The remaining terms express the gradient of the objective function with respect to the design variables which, after being numerically computed, can be used to drive any descent method to the optimal solution.

Most of the published works on the adjoint techniques are tailored to either structured or unstructured grids. Regardless of the discretization scheme, the grid type becomes important whenever the objective functional is a field integral; in this case, the functional gradient may include field integrals of the variations in nodal coordinates or other geometrical quantities. The standard way to compute these terms is by bifurcating one design variable at a time, defining the corresponding flow domain, remeshing it and numerically integrating over the grid nodes. However, such a treatment introduces inaccuracies and increases the computational cost. Recently, Jameson[15–17] proposed an adjoint formulation for inviscid flows with a unified gradient expression for structured and unstructured grids. The herein presented method is a much more general grid type independent formulation and, as it will be shown, is valid for both inviscid and viscous flows. Regardless of the objective functional used, which might be an either surface or boundary integral, the gradient expression consists only of surface integrals. The lack of field integrals is very advantageous in terms of both computational cost and gradient accuracy.

For the purpose of maximum generalization, the adjoint formulation if first presented for general pde's (hypothetical state equations), before specializing in the Navier–Stokes equations. The field integral of entropy generation, expressed in terms of temperature and velocity gradients, serves as objective function in problems targeting at the design of blades with minimum viscous losses. The adjoint formulation for the inverse design of blades is also presented in brief. Two turbomachinery applications are demonstrated; more applications, related to the design of isolated airfoils, ducts or turbomachinery blades, can be found in other publications[19–22] by the same authors.

2   GENERAL ADJOINT FORMULATION

Let us consider a domain $\Omega \in R^n$ (with coordinates $x_i, i = 1, ..., n$) and its boundary S; The shape of S, or a part of it, is determined by the vector of design variables b, associated with the parameterization scheme. Let us also consider that the governing (state) equations are first–order linear pde's in terms of the state variables U, namely

$$R_\Omega \; = \; E_i^\Omega \frac{\partial U}{\partial x_i} \; + \; H^\Omega U \; = \; 0 \tag{1}$$

for the interior of Ω and

$$R_S \; = \; E_i^S \frac{\partial U}{\partial x_i} \; + \; H^S U \; = \; 0 \tag{2}$$

along its boundary S. $E_i^\Omega, H^\Omega, E_i^S, H^S$ are independent of U. Our target is to find b that minimizes a functional $F(U)$ subject to eqs. (1) and (2). In general, F may consist of a field and a boundary integral,

$$F = F_\Omega + F_S = \int_\Omega \left(B_i^\Omega \frac{\partial U}{\partial x_i} + C^\Omega U \right) d\Omega + \int_S \left(B_i^S \frac{\partial U}{\partial x_i} + C^S U \right) dS \tag{3}$$

where $B_i^\Omega, C^\Omega, B_i^S, C^S$ are independent of U. Note that $x_i = x_i(b)$ and $U = U(x_i(b), b)$. The augmented functional is formed by introducing field and boundary *Lagrange* multipliers Ψ_Ω and Ψ_S,

$$F_{aug} \; = \; F_\Omega \; + \; F_S \; + \; \int_\Omega \Psi_\Omega R_\Omega d\Omega \; + \; \int_S \Psi_S R_S dS \tag{4}$$

and its variation with respect to the design variables yields

$$\begin{aligned}
\delta F_{aug} \; = \; & \int_\Omega \left[B_i^\Omega \delta \left(\frac{\partial U}{\partial x_i} \right) + C^\Omega \delta U \right] d\Omega + \int_\Omega \left(B_i^\Omega \frac{\partial U}{\partial x_i} + C^\Omega U \right) \delta(d\Omega) \\
+ \; & \int_S \left[B_i^S \delta \left(\frac{\partial U}{\partial x_i} \right) + C^S \delta U \right] dS + \int_S \left(B_i^S \frac{\partial U}{\partial x_i} + C^S U \right) \delta(dS) \\
+ \; & \int_\Omega \Psi_\Omega \left[E_i^\Omega \delta \left(\frac{\partial U}{\partial x_i} \right) + H^\Omega \delta U \right] d\Omega + \int_S \Psi_S \left[E_i^S \delta \left(\frac{\partial U}{\partial x_i} \right) + H^S \delta U \right] dS
\end{aligned} \tag{5}$$

Since

$$\delta U = \delta U(x_i(b), b) = \frac{\partial U}{\partial x_k} \delta x_k + \frac{\partial U}{\partial b} \delta b$$

its spatial derivative yields

$$\frac{\partial(\delta U)}{\partial x_i} = \frac{\partial^2 U}{\partial x_i \partial x_k} \delta x_k + \frac{\partial U}{\partial x_k} \frac{\partial(\delta x_k)}{\partial x_i} + \frac{\partial}{\partial x_i} \left(\frac{\partial U}{\partial b} \right) \delta b \tag{6}$$

3

Also

$$\delta\left(\frac{\partial U}{\partial x_i}\right) = \frac{\partial^2 U}{\partial x_i \partial x_k}\delta x_k + \frac{\partial}{\partial b}\left(\frac{\partial U}{\partial x_i}\right)\delta b \tag{7}$$

The last terms on the r.h.s. of eqs. (6) and (7) are equal so, by subtracting them, we get

$$\delta\left(\frac{\partial U}{\partial x_i}\right) = \frac{\partial(\delta U)}{\partial x_i} - \frac{\partial U}{\partial x_k}\frac{\partial(\delta x_k)}{\partial x_i} \tag{8}$$

Using eq. (8) and the Gauss' divergence theorem, terms such as $\int_\Omega B_i^\Omega \delta\left(\frac{\partial U}{\partial x_i}\right)d\Omega$, in eq. (5), can be transformed to

$$\int_\Omega B_i^\Omega \delta\left(\frac{\partial U}{\partial x_i}\right)d\Omega = \int_S B_i^\Omega \delta U n_i dS + \int_\Omega B_i^\Omega \frac{\partial^2 U}{\partial x_i \partial x_k}\delta x_k d\Omega - \int_S B_i^\Omega \frac{\partial U}{\partial x_k}\delta x_k n_i dS \tag{9}$$

Another "disturbing" field integral in eq. (5) is that depending on $\delta(d\Omega)$. The last term, which stands for the variation in "internal" finite volumes or areas due to boundary variations, will be analyzed on a 2D structured grid, using the associated metrics. However, the resulting expression is general and can be applied to either structured or unstructured, 2D or 3D, grids.

So, at a 2D structured grid node, $d\Omega = Jd\xi d\eta$, where $J = x_\xi y_\eta - x_\eta y_\xi$ is the Jacobian of the transformation. Since $d\xi$ and $d\eta$ are invariant quantities, $\delta(d\Omega) = (\delta J)d\xi d\eta$, where

$$\delta J = (\delta x)_\xi y_\eta + x_\xi(\delta y)_\eta - (\delta x)_\eta y_\xi - x_\eta(\delta y)_\xi$$

The relation between covariant and contravariant grid metrics gives

$$\delta J = J[(\delta x)_\xi \xi_x + (\delta x)_\eta \eta_x + (\delta y)_\xi \xi_y + (\delta y)_\eta \eta_y] = J[(\delta x)_x + (\delta y)_y]$$

or, in general

$$\delta(d\Omega) = \frac{\partial(\delta x_k)}{\partial x_k}d\Omega \tag{10}$$

Eq. (10) is metrics free and is, therefore, a general relation valid for both structured and unstructured grids.

Through eq. (10) and the Gauss' divergence theorem, the term $\int_\Omega B_i^\Omega \frac{\partial U}{\partial x_i}\delta(d\Omega)$ yields

$$\int_\Omega B_i^\Omega \frac{\partial U}{\partial x_i}\delta(d\Omega) = -\int_\Omega B_i^\Omega \frac{\partial^2 U}{\partial x_i \partial x_k}\delta x_k d\Omega + \int_S B_i^\Omega \frac{\partial U}{\partial x_i}\delta x_k n_k dS \tag{11}$$

By adding eqs. (9) and (11), so as to form (a part of) eq. (5), the two field integrals on their r.h.s. are eliminated. By further developing eq. (5), it takes the form

$$\delta F_{aug} \; = \; \underbrace{\int_{\Omega} \left(-E_i^{\Omega} \frac{\partial \Psi_{\Omega}}{\partial x_i} \; + \; H^{\Omega} \Psi_{\Omega} \; + \; C^{\Omega} \right) (\delta U \; - \; \frac{\partial U}{\partial x_k} \delta x_k) d\Omega}_{FAE}$$

$$+ \; \underbrace{\int_{S} \left(B_i^{S} \; + \; E_i^{S} \Psi_{S} \right) \frac{\partial (\delta U)}{\partial x_i} n_j dS}_{ABC} + \underbrace{\int_{S} \left(B_i^{\Omega} \; + \; E_i^{\Omega} \Psi_{\Omega} + C^{S} \; + \; H^{S} \Psi_{S} \right) \delta U n_i dS}_{ABC}$$

$$- \; \underbrace{\int_{S} B_i^{\Omega} \frac{\partial U}{\partial x_k} \delta x_k n_i dS}_{BSD} + \underbrace{\int_{S} B_i^{\Omega} \frac{\partial U}{\partial x_i} \delta x_k n_k dS}_{BSD} + \underbrace{\int_{S} C^{\Omega} U \delta x_k n_k dS}_{BSD}$$

$$- \; \underbrace{\int_{S} E_i^{\Omega} \Psi_{\Omega} \frac{\partial U}{\partial x_k} \delta x_k n_i dS}_{BSD} + \underbrace{\int_{S} B_i^{S} \frac{\partial U}{\partial x_i} \delta(dS)}_{BSD} \; + \; \underbrace{\int_{S} C^{S} U \delta(dS)}_{BSD} \tag{12}$$

After satisfying the *Field Adjoint Equation* (*FAE*) over Ω

$$- \; E_i^{\Omega} \frac{\partial \Psi_{\Omega}}{\partial x_i} \; + \; H^{\Omega} \Psi_{\Omega} \; + \; C^{\Omega} \; = \; 0 \tag{13}$$

and the *Adjoint Boundary Conditions* (*ABC*) over S

$$(B_i^{S} \; + \; E_i^{S} \Psi_{S}) \frac{\partial (\delta U)}{\partial x_i} n_j \; = \; 0$$

$$(B_i^{\Omega} \; + \; E_i^{\Omega} \Psi_{\Omega} \; + \; C^{S} \; + \; H^{S} \Psi_{S}) \delta U n_i \; = \; 0 \tag{14}$$

the remaining terms give the *Boundary Sensitivity Derivatives* (*BSD*)

$$\delta F_{aug} = \; - \; \int_{S} B_i^{\Omega} \frac{\partial U}{\partial x_k} \delta x_k n_i dS + \int_{S} B_i^{\Omega} \frac{\partial U}{\partial x_i} \delta x_k n_k dS + \int_{S} C^{\Omega} U \delta x_k n_k dS$$

$$- \; \int_{S} E_i^{\Omega} \Psi_{\Omega} \frac{\partial U}{\partial x_k} \delta x_k n_i dS + \int_{S} B_i^{S} \frac{\partial U}{\partial x_i} \delta(dS) \; + \; \int_{S} C^{S} U \delta(dS) \tag{15}$$

Further development of eq. (15) so as to derive the gradient of F (or F_{aug}) with respect to b, depends on the chosen parameterization.

The presence of nonlinearities, in either the state equations or F, is not a problem at all. For instance, by adding an extra field integral such as

$$F_n = \int_{\Omega} G_{ij}^{\Omega} \frac{\partial U}{\partial x_i} \frac{\partial U}{\partial x_j} d\Omega \tag{16}$$

to the objective function, eq. (3), its variation is written as

$$\delta F_n = \int_{\Omega} G_{ij}^{\Omega} \delta(\frac{\partial U}{\partial x_i}) \frac{\partial U}{\partial x_j} d\Omega + \int_{\Omega} G_{ij}^{\Omega} \frac{\partial U}{\partial x_i} \delta(\frac{\partial U}{\partial x_j}) d\Omega + \int_{\Omega} G_{ij}^{\Omega} \frac{\partial U}{\partial x_i} \frac{\partial U}{\partial x_j} \frac{\partial (\delta x_k)}{\partial x_k} d\Omega$$

or

$$
\begin{aligned}
\delta F_n \;=\; & -2 \underbrace{\int_\Omega G_{ij}^\Omega \frac{\partial^2 U}{\partial x_j \partial x_i}(\delta U - \frac{\partial U}{\partial x_k}\delta x_k)d\Omega}_{FAE} \\
& + \underbrace{\int_S G_{ij}^\Omega \delta U \frac{\partial U}{\partial x_j}n_i dS}_{ABC} + \underbrace{\int_S G_{ij}^\Omega \delta U \frac{\partial U}{\partial x_i}n_j dS}_{ABC} \\
& - \underbrace{\int_S G_{ij}^\Omega \frac{\partial U}{\partial x_k}\frac{\partial U}{\partial x_j}\delta x_k n_i dS}_{BSD} - \underbrace{\int_S G_{ij}^\Omega \frac{\partial U}{\partial x_k}\frac{\partial U}{\partial x_i}\delta x_k n_j dS}_{BSD} + \underbrace{\int_S G_{ij}^\Omega \frac{\partial U}{\partial x_i}\frac{\partial U}{\partial x_j}\delta x_k n_k dS}_{BSD} \quad (17)
\end{aligned}
$$

with evident contributions to the field and boundary adjoint equations as well as the functional gradient; note that the latter includes only boundary integrals.

Similarly, in the presence of any second–order term, the variation in the second–order derivative should be transformed to the second–order derivative of the variation. By computing the second–order derivative of δU

$$
\begin{aligned}
\frac{\partial^2(\delta U)}{\partial x_i \partial x_j} \;=\; & \frac{\partial^2}{\partial x_i \partial x_j}(\frac{\partial U}{\partial b})\delta b \;+\; \frac{\partial^3 U}{\partial x_i \partial x_j \partial x_k}\delta x_k \;+\; \frac{\partial^2 U}{\partial x_i \partial x_k}\frac{\partial(\delta x_k)}{\partial x_j} \\
& + \frac{\partial^2 U}{\partial x_j \partial x_k}\frac{\partial(\delta x_k)}{\partial x_i} \;+\; \frac{\partial U}{\partial x_k}\frac{\partial^2(\delta x_k)}{\partial x_i \partial x_j}
\end{aligned}
$$

the variation in the second–order derivative

$$
\delta(\frac{\partial^2 U}{\partial x_i \partial x_j}) \;=\; \frac{\partial^3 U}{\partial x_i \partial x_j \partial x_k}\delta x_k \;+\; \frac{\partial}{\partial b}(\frac{\partial^2 U}{\partial x_i \partial x_j})\delta b
$$

and eliminating the common terms, we get

$$
\delta(\frac{\partial^2 U}{\partial x_i \partial x_j}) \;=\; \frac{\partial^2(\delta U)}{\partial x_i \partial x_j} - \frac{\partial^2 U}{\partial x_i \partial x_k}\frac{\partial(\delta x_k)}{\partial x_j} - \frac{\partial^2 U}{\partial x_j \partial x_k}\frac{\partial(\delta x_k)}{\partial x_i} - \frac{\partial U}{\partial x_k}\frac{\partial^2(\delta x_k)}{\partial x_i \partial x_j} \quad (18)
$$

By means of eq. (18) and the Gauss' divergence theorem, the second–order adjoint equations and boundary conditions can be derived.

3 AERODYNAMIC SHAPE OPTIMIZATION

3.1 Flow Equations

The state equations in vector form for a compressible fluid flow, (i=1,2 in 2D and i=1,2,3 in 3D), are

$$
\vec{R}(\vec{U}, x_k, b) = \frac{\partial \vec{U}}{\partial t} + \frac{\partial \vec{f}_i^{inv}}{\partial x_i} - \frac{\partial \vec{f}_i^{vis}}{\partial x_i} = \vec{0} \quad (19)
$$

where x_k stand for the Cartesian coordinates and $\vec{U} = \left[\rho, \vec{V}, E\right]^T$ is the vector of conservative variables, $\vec{V}$ is the velocity and $E = \rho e + \frac{1}{2}\rho u_i^2$ is the total energy per unit volume. The inviscid and viscous fluxes are given by

$$\vec{f}_i^{inv} = \begin{bmatrix} \rho u_i \\ \rho u_i \vec{V} + p\vec{\delta}_i \\ u_i(E + p) \end{bmatrix} \ , \ \vec{f}_i^{vis} = \begin{bmatrix} 0 \\ \vec{\tau}_i \\ u_j\tau_{ij} + q_i \end{bmatrix} \tag{20}$$

where $\vec{\tau}_i$ are the viscous stresses, with

$$\tau_{ij} = \mu(\frac{\partial u_i}{\partial x_j} + \frac{\partial u_j}{\partial x_i}) + \lambda\delta_{ij}\frac{\partial u_k}{\partial x_k} \ , \quad \lambda = -\frac{2}{3}\mu \tag{21}$$

$\vec{\delta}_i$, δ_{ij} are the Kronecker symbols and $q_i = k\frac{\partial T}{\partial x_i}$.

3.2   Objective Functionals

Inverse design problems in which a desirable pressure distribution over the blade surfaces S_w (or a part of it) is specified can be handled through the standard objective functional

$$F = \frac{1}{2}\int_{S_w}(p - p_{tar})^2 dS \tag{22}$$

In this case, it is convenient that F is defined over the part of the domain boundary that is also associated with the shape parameterization. The corresponding development has been presented elsewhere[19] and will be omitted in the interest of space. Thanks to the theory presented in the previous section, the gradient of F is free of field integrals.

The objective functional[19] that is also used in this paper is a field integral expressing the viscous losses due to the boundary layer formation. It is written in terms of entropy s generation as

$$F = \int_{\Omega}\rho u_i\frac{\partial s}{\partial x_i}d\Omega \tag{23}$$

It can be shown that eq. (23) is equivalent to the difference in mass averaged entropy s between the inlet to and the outlet from the flow domain. Note that eq. (23) is restricted only to profile losses in a cascade of duct. According to Denton,[18] who used eq. (23) to estimate losses in cascade flows, F is also expressed in terms of temperature and velocity gradients as

$$F = \int_{\Omega}\frac{\tau_{ij}}{T}\frac{\partial u_i}{\partial x_j}d\Omega \tag{24}$$

and, after using eqs. (8) and (10) while assuming that the spatial derivatives of the viscosity coefficient are negligible, its variation reads

$$\delta F = \ - \ \int_{\Omega}\frac{\tau_{ij}}{T^2}\frac{\partial u_i}{\partial x_j}\left(\delta T - \frac{\partial T}{\partial x_k}\delta x_k\right)d\Omega - 2\int_{\Omega}\frac{\partial}{\partial x_j}\left(\frac{\tau_{ij}}{T}\right)\left(\delta u_i - \frac{\partial u_i}{\partial x_k}\delta x_k\right)d\Omega$$

$$ - \ 2\int_{S_w}\frac{\tau_{ij}}{T}\frac{\partial u_j}{\partial x_k}n_i\delta x_k dS + \int_{S_w}\frac{\tau_{ij}}{T}\frac{\partial u_i}{\partial x_j}\delta x_k n_k dS \tag{25}$$

3.3 The Adjoint Problem

The variation in the augmented objective functional reads

$$\delta F_{aug} = \delta F + \int_{\Omega} \vec{\Psi}^T \delta \left(\frac{\partial \vec{f}_i^{inv}}{\partial x_i} - \frac{\partial \vec{f}_i^{vis}}{\partial x_i} \right) d\Omega \tag{26}$$

where

$$\int_{\Omega} \vec{\Psi}^T \delta \left(\frac{\partial \vec{f}_i^{inv}}{\partial x_i} \right) d\Omega = - \int_{\Omega} \left(\delta \vec{U}^T - \frac{\partial \vec{U}}{\partial x_k}^T \delta x_k \right) \left(A_i^T \frac{\partial \vec{\Psi}}{\partial x_i} \right) d\Omega$$

$$+ \int_{\Omega} \vec{\Psi}^T \frac{\partial}{\partial x_k} \left(\frac{\partial \vec{f}_i^{inv}}{\partial x_i} \right) \delta x_k d\Omega - \int_{S_w} \frac{\partial \vec{U}}{\partial x_k}^T A_n^T \vec{\Psi} \delta x_k dS + \int_{S_w} \Psi_{i+1} n_i \delta p dS$$

$$+ \int_{S_w} (\Psi_{i+1} p - \vec{\Psi}^T \vec{f}_i^{inv}) \delta(n_i dS) + \int_{S_{i,o}} \delta \vec{U}^T (A_n^T \vec{\Psi}) dS \tag{27}$$

and[19]

$$\int_{\Omega} \vec{\Psi}^T \delta \left(\frac{\partial \vec{f}_i^{vis}}{\partial x_i} \right) d\Omega =$$

$$- \int_{\Omega} \left(\delta \vec{U} - \frac{\partial \vec{U}}{\partial x_k} \delta x_k \right)^T \left(A_i^T \frac{\partial \vec{\Psi}}{\partial x_i} \right) d\Omega - \int_{\Omega} \left(\delta \vec{W} - \frac{\partial \vec{W}}{\partial x_k} \delta x_k \right)^T \vec{K} d\Omega$$

$$+ \int_{\Omega} \vec{\Psi}^T \frac{\partial}{\partial x_k} \left(\frac{\partial \vec{f}_i^{inv}}{\partial x_i} - \frac{\partial \vec{f}_i^{vis}}{\partial x_i} \right) \delta x_k d\Omega - \int_{S_w} \frac{\partial \vec{U}}{\partial x_k}^T (A_i^T n_i) \vec{\Psi} \delta x_k dS$$

$$+ \int_{S_w} \Psi_i n_i \delta p dS + \int_{S_w} (\Psi_i p - \vec{\Psi}^T \vec{f}_i^{vis}) \delta(n_i dS) + \int_{S_{i,o}} \delta \vec{U}^T (A_n^T \vec{\Psi}) dS +$$

$$+ \int_{S_w} \delta u_i \left[\mu \left(\frac{\partial \Psi_{j+1}}{\partial x_i} + u_j \frac{\partial \Psi_m}{\partial x_i} + \frac{\partial \Psi_{i+1}}{\partial x_j} + u_i \frac{\partial \Psi_m}{\partial x_j} \right) + \lambda \delta_{ij} \left(\frac{\partial \Psi_{k+1}}{\partial x_k} + u_k \frac{\partial \Psi_m}{\partial x_k} \right) - \Psi_m \tau_{ij} \right] n_j dS$$

$$+ \int_{S_w} \delta T \left(k \frac{\partial \Psi_m}{\partial x_i} n_i \right) dS - \int_{S_w} \Psi_m \delta(q_j n_j dS) + \int_{S_w} \Psi_m q_j \delta(n_j dS)$$

$$- \int_{S_w} \frac{\Psi_{i+1}}{n_i} [\delta \tau_{ij} n_i n_j + \tau_{ij} \delta(n_i n_j)] dS + \int_{S_w} \frac{\Psi_{i+1}}{n_i} \tau_{ij} \delta(n_i n_j) dS - \int_{S_w} u_i \Psi_m \delta \tau_{ij} n_j dS$$

$$- \int_{S_w} \frac{\partial u_i}{\partial x_l} \left[\mu \left(\frac{\partial \Psi_{j+1}}{\partial x_i} + u_j \frac{\partial \Psi_m}{\partial x_i} + \frac{\partial \Psi_{i+1}}{\partial x_j} + u_i \frac{\partial \Psi_m}{\partial x_j} \right) + \lambda \delta_{ij} \left(\frac{\partial \Psi_{k+1}}{\partial x_k} + u_k \frac{\partial \Psi_m}{\partial x_k} \right) \right] \delta x_l n_j dS$$

$$+ \int_{S_w} \frac{\partial T}{\partial x_k} \left(k \frac{\partial \Psi_m}{\partial x_i} \right) \delta x_k n_i dS - \int_{S_w} \left(\vec{\Psi}^T \frac{\partial \vec{f}_i^{vis}}{\partial x_k} \right) \delta x_k n_i dS \tag{28}$$

where $m = 4$ for 2D flows and $m = 5$ for 3D flows. The variation in F_{aug} is finally written as

8

$$
\begin{aligned}
\delta F_{aug} = & -\underbrace{\int_{\Omega} \frac{\tau_{ij}}{T^2} \frac{\partial u_i}{\partial x_j} \left(\delta T - \frac{\partial T}{\partial x_k} \delta x_k \right) d\Omega}_{FAE} - \underbrace{2 \int_{\Omega} \frac{\partial}{\partial x_j} \left(\frac{\tau_{ij}}{T} \right) \left(\delta u_i - \frac{\partial u_i}{\partial x_k} \delta x_k \right) d\Omega}_{FAE} \\
& - \underbrace{2 \int_{S_w} \frac{\tau_{ij}}{T} \frac{\partial u_j}{\partial x_k} n_i \delta x_k dS}_{BSD} + \underbrace{\int_{S_w} \frac{\tau_{ij}}{T} \frac{\partial u_i}{\partial x_j} \delta x_k n_k dS}_{BSD} - \underbrace{\int_{S_w} \frac{\partial \vec{U}}{\partial x_k}^T (A_i^T n_i) \vec{\Psi} \delta x_k dS}_{BSD} \\
& - \underbrace{\int_{\Omega} \left(\delta \vec{U} - \frac{\partial \vec{U}}{\partial x_k} \delta x_k \right)^T \left(A_i^T \frac{\partial \vec{\Psi}}{\partial x_i} \right) d\Omega}_{FAE} - \underbrace{\int_{\Omega} \left(\delta \vec{W} - \frac{\partial \vec{W}}{\partial x_k} \delta x_k \right)^T \vec{K} d\Omega}_{FAE} \\
& + \underbrace{\int_{S_w} \Psi_i n_i \delta p dS}_{BCW} + \underbrace{\int_{S_w} (\Psi_i p - \vec{\Psi}^T \vec{f}_i^{inv}) \delta(n_i dS)}_{BSD} + \underbrace{\int_{S_{i,o}} \delta \vec{U}^T (A_n^T \vec{\Psi}) dS}_{BCIO} + \\
& + \underbrace{\int_{S_w} \delta T \left(k \frac{\partial \Psi_m}{\partial x_i} n_i \right) dS}_{BCW} - \underbrace{\int_{S_w} \Psi_m \delta(q_j n_j dS)}_{BCW} + \underbrace{\int_{S_w} \Psi_m q_j \delta(n_j dS)}_{BSD} \\
& - \underbrace{\int_{S_w} \frac{\Psi_{i+1}}{n_i} [\delta \tau_{ij} n_i n_j + \tau_{ij} \delta(n_i n_j)] dS}_{BCW} + \underbrace{\int_{S_w} \frac{\Psi_{i+1}}{n_i} \tau_{ij} \delta(n_i n_j) dS}_{BSD} - \underbrace{\int_{S_w} u_i \Psi_m \delta \tau_{ij} n_j dS}_{BCW} \\
& - \underbrace{\int_{S_w} \frac{\partial u_i}{\partial x_l} \left[\mu \left(\frac{\partial \Psi_{j+1}}{\partial x_i} + u_j \frac{\partial \Psi_m}{\partial x_i} + \frac{\partial \Psi_{i+1}}{\partial x_j} + u_i \frac{\partial \Psi_m}{\partial x_j} \right) + \lambda \delta_{ij} \left(\frac{\partial \Psi_{k+1}}{\partial x_k} + u_k \frac{\partial \Psi_m}{\partial x_k} \right) \right] \delta x_l n_j dS}_{BSD} \\
& + \underbrace{\int_{S_w} \frac{\partial T}{\partial x_k} \left(k \frac{\partial \Psi_m}{\partial x_i} \right) \delta x_k n_i dS}_{BSD} - \underbrace{\int_{S_w} \left(\vec{\Psi}^T \frac{\partial \vec{f}_i^{vis}}{\partial x_k} \right) \delta x_k n_i dS}_{BSD} \quad (29)
\end{aligned}
$$

The *Field Adjoint Equations* (FAE) are written as

$$
\frac{\partial \vec{\Psi}}{\partial t} - A_i^T \frac{\partial \vec{\Psi}}{\partial x_i} - M^{-T} \vec{K} - M^{-T} \vec{L} = \vec{0} \quad (30)
$$

where $\vec{K} = (K_1, K_{r+1}, K_m)^T$, $\vec{L} = (L_1, L_{r+1}, L_m)^T$, $r = 1, 2(3)$, and

$$
K_1 = -\frac{T}{\rho} \frac{\partial}{\partial x_i} \left(k \frac{\partial \Psi_m}{\partial x_i} \right)
$$

$$
K_{r+1} = \frac{\partial}{\partial x_j} \left[\mu \left(\frac{\partial \Psi_{j+1}}{\partial x_r} + u_j \frac{\partial \Psi_m}{\partial x_r} + \frac{\partial \Psi_{r+1}}{\partial x_j} + u_r \frac{\partial \Psi_m}{\partial x_j} \right) + \lambda \delta_{rj} \left(\frac{\partial \Psi_{k+1}}{\partial x_k} + u_k \frac{\partial \Psi_m}{\partial x_k} \right) \right] - \tau_{rj} \frac{\partial \Psi_m}{\partial x_j}
$$

$$
K_m = \frac{T}{p} \frac{\partial}{\partial x_i} \left(k \frac{\partial \Psi_m}{\partial x_i} \right)
$$

$$L_1 = \frac{1}{T^2} \tau_{ij} \frac{\partial u_i}{\partial x_j} \left(-\frac{p}{\rho^2(\gamma - 1)} \right)$$

$$L_{r+1} = 2 \frac{\partial}{\partial x_j} \left(\frac{\mu}{T} \tau_{rj} \right)$$

$$L_m = \frac{1}{T^2} \tau_{ij} \frac{\partial u_i}{\partial x_j} \frac{1}{\rho(\gamma - 1)}$$

Along the solid walls, homogeneous Dirichlet conditions are imposed for Ψ_{r+1}. Also $\Psi_m = 0$ for constant wall temperature, or $\frac{\partial \Psi_m}{\partial n} = 0$ for adiabatic walls (terms marked with BCW). The inlet, outlet conditions (BCIO) are defined so as to eliminate $\delta \vec{U}^T (A_n^T \vec{\Psi}) = 0$. The remaining terms (BSD) provide the objective function gradient as follows

$$
\begin{aligned}
\delta F_{aug} &= -\int_{S_w} \left(\vec{\Psi}^T \vec{f}_i^{inv} \right) \delta(n_i dS) - \int_{S_w} \frac{\partial \vec{U}}{\partial x_k}^T (A_i^T n_i) \vec{\Psi} \delta x_k dS + \\
&\quad \int_{S_w} \left(\vec{\Psi}^T \frac{\partial \vec{f}_i^{vis}}{\partial x_k} \right) \delta x_k n_i dS + \int_{S_w} \Psi_4 q_j \delta(n_j dS) - \\
&\quad \int_{S_w} \frac{\partial u_i}{\partial x_l} \left[\mu \left(\frac{\partial \Psi_{j+1}}{\partial x_i} + u_j \frac{\partial \Psi_m}{\partial x_i} + \frac{\partial \Psi_{i+1}}{\partial x_j} + u_i \frac{\partial \Psi_m}{\partial x_j} \right) \right. \\
&\quad + \left. \lambda \delta_{ij} \left(\frac{\partial \Psi_{k+1}}{\partial x_k} + u_k \frac{\partial \Psi_m}{\partial x_k} \right) \right] \delta x_l n_j dS - \\
&\quad 2 \int_{S_w} \tau_{ij} \frac{\partial u_j}{\partial x_k} n_i \delta x_k dS + \int_{S_w} \frac{1}{T} \tau_{ij} \frac{\partial u_i}{\partial x_j} \delta x_k n_k dS
\end{aligned}
\tag{31}
$$

which is independent of field integrals, although the functional was, in fact, a field integral.

4 METHOD APPLICATION

4.1 Inverse Design of a Symmetric Cascade–Inviscid Flow

The first problem is concerned with the inverse design of a symmetric cascade at zero stagger angle, fig. (1) The flow is considered to be inviscid with axial inlet flow and exit isentropic Mach number equal to $M_{2,is} = 0.3$. The airfoil is parameterized using seven Bezier control points per side, including the leading and trailing edges. The chordwise locations of all control points are fixed and symmetric around midchord. A coarse 61×21 H-type structured grid is used.

A target pressure distribution is defined over the airfoil contour and the objective function is that of eq. (22) The target pressure distribution was created beforehand, by solving the Euler equations for a cascade with a known airfoil shape created using the same parameterization scheme. Iso–Mach contours and grid within the target geometry are shown in fig. 1, left.

The objective function gradient values obtained for the initial airfoil are compared with the outcome of central finite–differences, which are considered to give "reference" values for the gradient components. With five degrees of freedom (i.e. the pitchwise coordinate of the five internal control points for the one of the sides of the symmetric airfoil), the finite–difference computation required $2 \times 5 = 10$ flow analyses. The design variable value increment ($\pm\epsilon$ in the central–difference quotient) was set to 10^{-7} and the flow solver was allowed to converge up to machine accuracy, with double precision calculations. The comparison shown in fig. 1, right, is excellent.
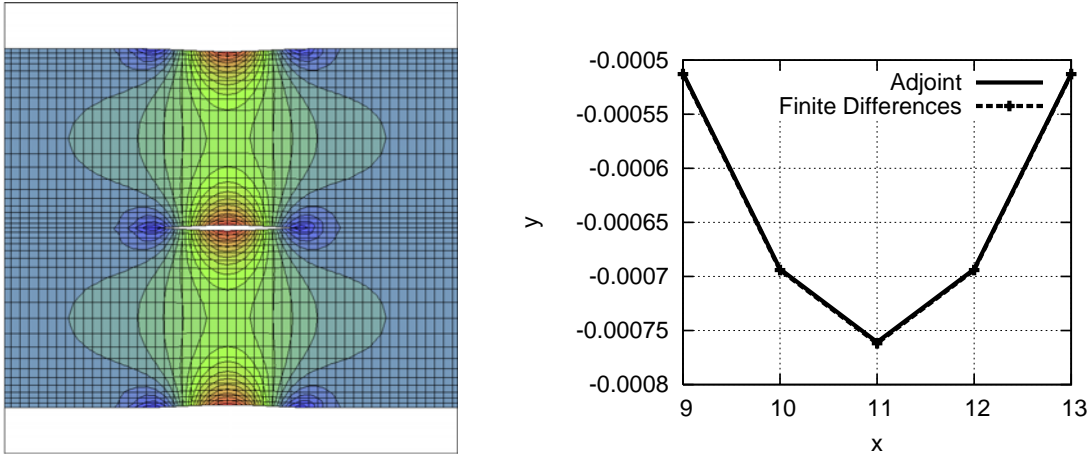
Figure 1: Inverse Design of a 2D Cascade–Inviscid Flow. Left: Iso–Mach contours and grid in the targeted geometry. Right: Objective function gradient values obtained using the present adjoint formulation and a central finite–difference scheme, for the initial airfoil shape.

The convergence of the objective function value is shown in fig. 2, left. Three different algorithms are used: the steepest descent algorithm with constant stepsize $\eta = 100$, the Fletcher–Reeves conjugate gradient algorithms with $\eta = 100$ and the BFGS quasi–Newton algorithm with $\eta = 1$. In fig. 2, right, the reference, initial and optimal control points are shown using the three aforementioned algorithms.

From fig. 2, we conclude that all three algorithms converge to the global optimal solution. However, the superiority of QN over the other two and of CG over SD are obvious. BFGS converges to machine accuracy (the cost function value is lowered to 10^{-20}) in 45 cycles only. CG lowers the cost function value by eight orders in 100 cycles but, after the $40th$ cycle, its convergence becomes dramatically slow. SD requires 40 cycles before stagnating at 10^{-10} (starting from a cost of about 10^{-5}). Fig. 2, right, shows the optimal control points computed after 100 cycles. Despite the different convergence level, the finally computed airfoils are almost identical or, at least, without visible differences. The reference control points' error which refer to the global optimum are equal to 10^{-8}, 10^{-3}, 10^{-2} for
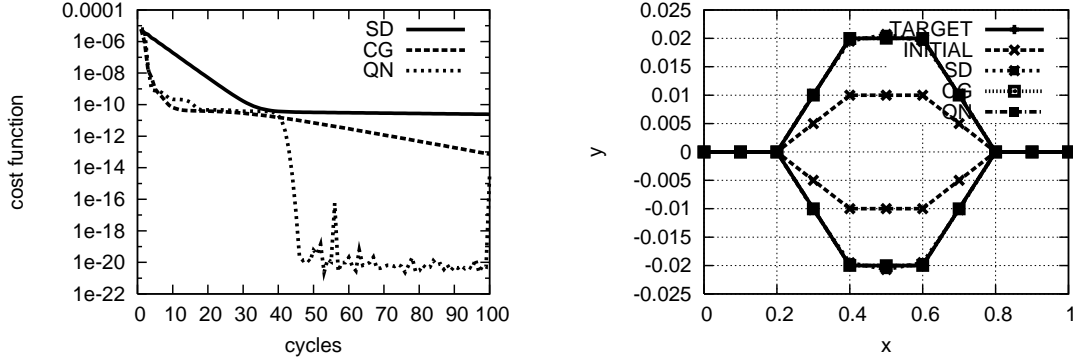
Figure 2: Inverse Design of a 2D Cascade–Inviscid Flow. Left: Convergence of the objective function using the Steepest–Descent (SD), the Fletcher–Reeves Conjugate–Gradient (CG) and the BFGS Quasi–Newton (QN) algorithms. Right: Reference, initial and optimal Bezier control points. Symmetry across the horizontal and vertical mid–axis can be seen.

the three methods, respectively (with the same CPU cost).

Due to both chordwise and pitchwise symmetry, the design variables can reduce to three. However, for better visualizing the convergence behavior of the optimization algorithms, we selected only two of them as design variables while the third one took on its reference value. Using the three aforementioned algorithms the solution paths are shown in fig. 3. The shape of the iso–cost curves on the design variable space, which directly determines the direction and value of the cost function gradient, explains the different convergence behaviours of the three methods tested.
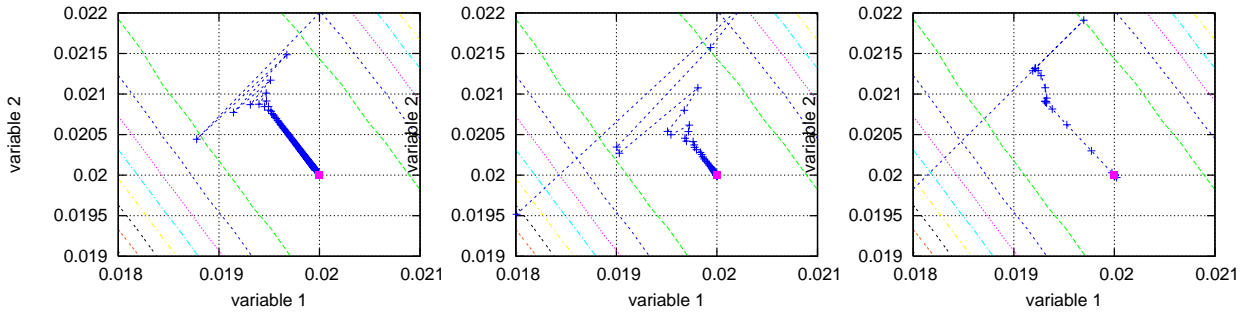
Figure 3: Inverse Design of a 2D Cascade–Inviscid Flow. Solution path plotted on the design variables' space using the Steepest–Descent (SD), left, the Fletcher–Reeves Conjugate–Gradient (CG), middle and the BFGS Quasi–Newton (QN), right, algorithms. Iso–cost curves are also plotted.

According to these figures, QN and CG converge to the global optimum (machine accuracy) in 23 and 90 cycles respectively, whereas SD reduces the cost function value by 7 orders in 100 cycles and continues to drift slowly. The SD convergence rate cannot be

12

improved by just increasing the stepsize, as shown by computational experiments (not shown here).

4.2 Optimization of a 3D Compressor Cascade–Losses Minimization

The design of optimal compressor blades for a 3D peripheral cascade, aiming at minimum entropy generation due to profile losses within the flow passage is the second problem to be presented. The isentropic exit Mach number is 0.42, the inlet flow angles are 50° (peripheral) and 0° (radial) and the chord–based Reynolds number is 10^5. The cascade has a (radially constant) stagger angle of 29 deg. An H–type structured grid of 745.855 nodes is used, generated through elliptic equations. Turbulence is modeled using the Spalart–Allmaras model; the variation in turbulent viscosity, during the adjoint formulation, is however neglected.

The blade pressure and suction sides are parameterized using NURBS functions with 13 control points in the longitudinal direction and 5 in the radial one. Only the control points placed along the hub and tip are directly controlled. The interior control points in the spanwise direction are obtained by linearly interpolating between those at the hub and tip. Among all control points, only the peripheral coordinates are free to vary. The final number of the free variables to be optimized is equal to 28. Constraints are imposed with respect to the minimum allowed blade thickness t_i at n locations .

The algorithm converges in 40 cycles. Fig. 4, left, shows the evolution of the entropy generation value during the cycles, which, as expected, presents some oscillations during the first cycles since some infeasible shapes (i.e. thin blades) are produced. This can be explained by examining fig. 4, right, where the sum of values of the violated geometrical constraint values $\sum_{i=1,n} max(\tilde{t}_i - t_i, 0)$ is plotted. During the first cycles, the violation of the constraints is frequent. Afterwards, close to convergence, some slight violations of the constraints that inevitably appear can be neglected.

As a consequence of the minimization of entropy generation, the total pressure loss coefficient in the cascade reduces from $\omega = 0.032$ to $\omega = 0.023$. This noticeable improvement (28%) can be attributed to the fact that the imposed constraints practically allowed a "reasonable" reduction in blade thickness (10% reduction compared to the initial blade). The pressure distribution over a part of the peripheral cascade is illustrated in fig 5, right.

The initial and optimal set of control points and the blade contours for the blade hub, fig. 6, and tip airfoils, fig. 7, are also shown. These figures reveal the same tendency for the blade geometry and control points. The blade contour slope right after the leading edge becomes milder and the blade tends to become thinner; however any further reduction in its thickness is avoided due to the constraint imposition.
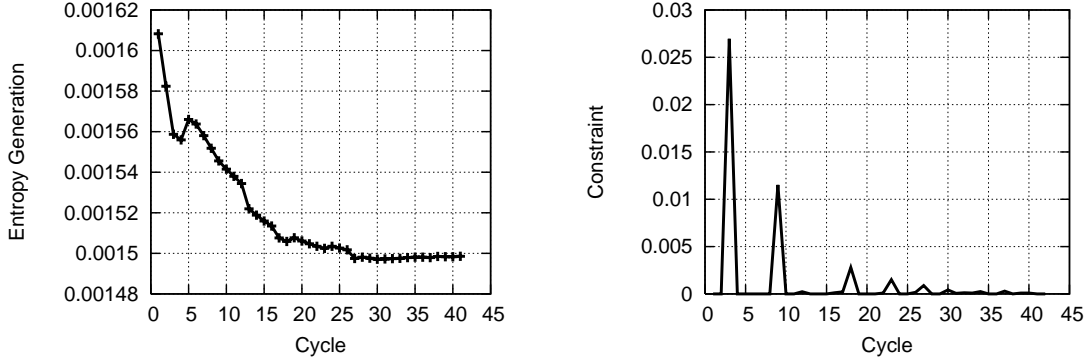
Figure 4: Optimization of a 3D Compressor Cascade. Left: Convergence of entropy generation rate. Right: Sum of geometrical constraints, $\sum_{i=1,n} max(\tilde{t}_i - t_i, 0)$, quantifying the violation of constraints at each cycle.
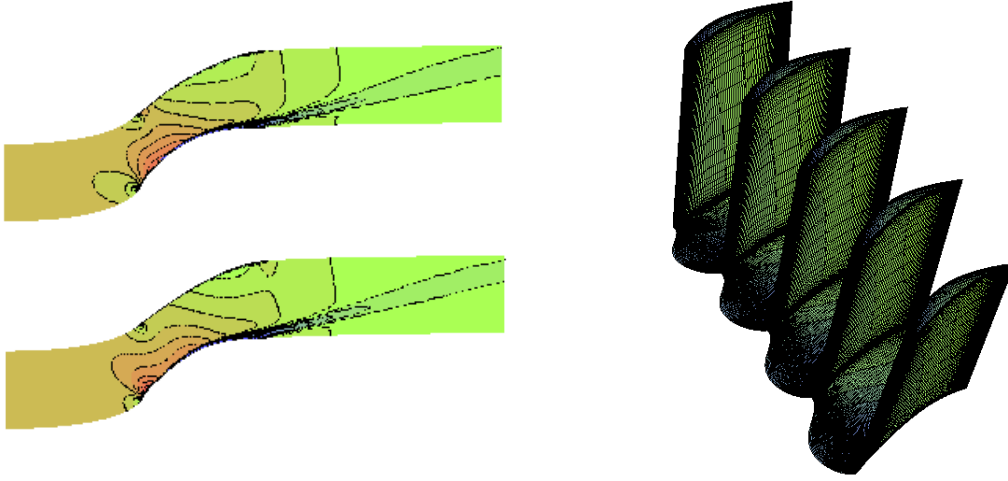
Figure 5: Optimization of a 3D Compressor Cascade. Left: Mach number distribution for the initial (top) and the optimal (bottom) blade at midspan. Maximum Mach=0.95, increment=0.0475. 3D computational grid and pressure distribution over the blade and hub surfaces of the optimal peripheral cascade. Minimum P=1.4bar, maximum P=2.5bar, increment=0.055bar.

Comments on the convergence trend of the optimization algorithm and the physical meaning of the final solution can be given using fig. 8. The derivatives of the objective functional F measuring the entropy generation with respect to the NURBS control points of the suction side, are positive at both hub and tip (14 first values); in contrast, the corresponding derivatives for the pressure side control points are negative. Thus, generally, the blade tends to become thinner. Higher gradient values are computed next to the leading edge, on both sides, so the front part of the blade tends to become quite thin. Since, however, the optimization method is constrained by the minimum blade thickness, the constraint imposition finally leads to a blade of reasonable thickness.

14
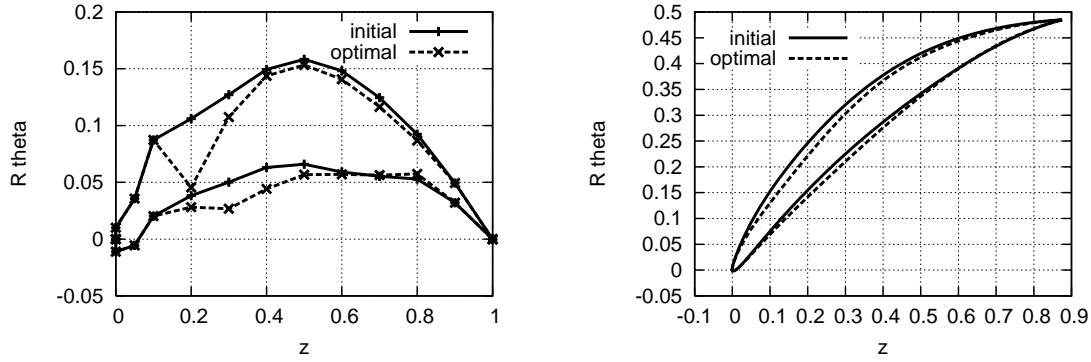
Figure 6: Optimization of a 3D Compressor Cascade. Initial and optimal control points and blade contours for the blade hub.
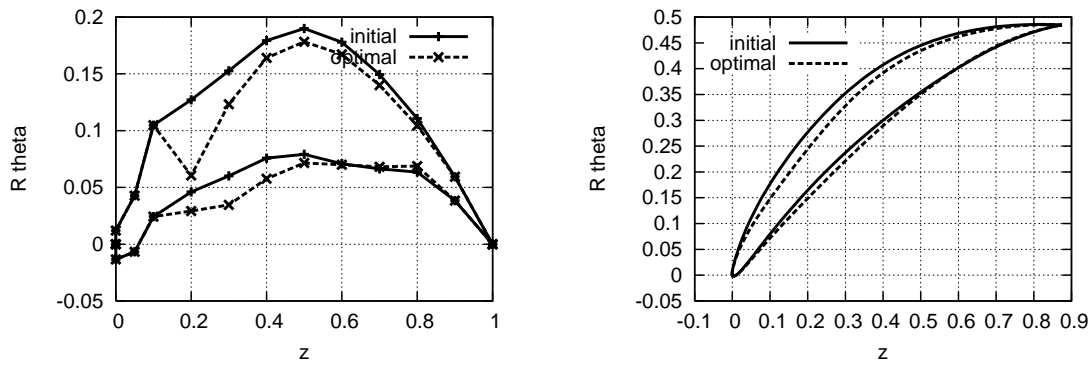
Figure 7: Optimization of a 3D Compressor Cascade. Initial and optimal control points and blade contours for the blade tip.
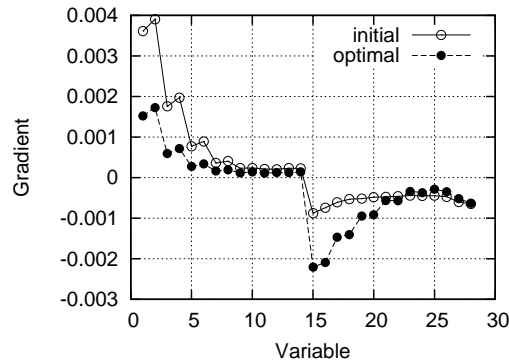
Figure 8: Optimization of a 3D Compressor Cascade. Objective functional gradient components corresponding to each one of the design variables. The first 14 variables parameterize the suction side (7 for the tip and 7 for the hub). The remaining ones correspond to the pressure side.

5 CONCLUSIONS

The continuous adjoint formulation for aerodynamic shape optimization problems was presented in a grid type independent manner. Even if the objective functional was a field integral, such as the one used for designing cascades (or ducts) with minimum entropy generation due to viscous losses, the expressions for its gradient with respect to the design variables are surface integrals. The advantage is important: the gradient is computed without the extra numerical error caused by field integrals and without extra computational cost due to remeshing, etc. The presented formulation is general and can be extended, apart from fluid flow applications, to any problem for which the state equations are linear or nonlinear pde's of any order and for any integral objective functional, as clearly shown above.

ACKNOWLEDGEMENTS

REFERENCES

[1] J.L. Lions. Optimal control of systems governed by partial differential equations. Springer-Verlag, New York, 1971.

[2] O. Pironneau. Optimal shape design for elliptic systems. Springer-Verlag, New York, 1984.

[3] A. Jameson. Aerodynamic Design via Control Theory. Journal of Scientific Computing, 3, 233-260, 1988.

[4] A. Jameson and J. Reuther. Control Theory Based Airfoil Design using the Euler Equations. AIAA Paper 94-4272-CP, 1994.

[5] A. Jameson. Optimum Aerodynamic Design using CFD and Control Theory. AIAA Paper 95-1729, AIAA 12th Computational Fluid Dynamics Conference, San Diego, June 1995.

[6] J.J. Alonso and I.M. Kroo and A. Jameson. Advanced Algorithms for Design and Optimization of Quiet Supersonic Platform. AIAA-2002-0144, AIAA 40th Aerospace Sciences Meeting and Exhibit, Reno NV, January 2002.

[7] S. Nadarajah and A. Jameson and J.J. Alonso. An Adjoint Method for the Calculation of Remote Sensitivities in Supersonic Flow. AIAA-2002-0261, AIAA 40th Aerospace Sciences Meeting and Exhibit, Reno NV, January 2002.

[8] A. Jameson and N. Pierce and L. Martinelli. Optimum Aerodynamic Design using the Navier-Stokes Equations. Theoretical and Computational Fluid Dynamics, 10, 213-237, 1998.

[9] J. Reuther and J.J. Alonso and M.J. Rimlinger and A. Jameson. Aerodynamic Shape Optimization of Supersonic Aircraft Configurations via an adjoint formulation on distributed memory parallel computers. Journal of Computers and Fluids, 28, 675-700, 1999.

[10] M. Harbeck and A. Jameson. Exploring the Limits of Transonic Shock-free Airfoil Design. 43rd AIAA Aerospace Sciences Meeting and Exhibit, AIAA Paper 2005-1041, Reno, NV, January 10-13, 2005.

[11] M.B. Giles. Discrete adjoint approximations with shocks. Journal of Hyperbolic Problems: Theory, Numerics, Applications, 2003.

[12] M.C. Duta and M.B. Giles and M.S. Campobasso. The harmonic adjoint approach to unsteady turbomachinery design. International Journal for Numerical Methods in Fluids, 40(3-4), 323-332, 2002.

[13] M.S. Campobasso and M.C. Duta and M.B. Giles. Adjoint calculation of sensitivities of turbomachinery objective functions. AIAA Journal of Propulsion and Power, 19(4), 2003.

[14] M.S. Campobasso and M.C. Duta and M.B. Giles. Adjoint methods for turbomachinery design. ISOABE Conference, 2001.

[15] A. Jameson and S. Kim. Reduction of the Adjoint Gradient Formula in the Continous Limit. AIAA-2003-0040, AIAA 41th Aerospace Sciences Meeting and Exhibit, Reno NV, January 2003.

[16] S. Kim and K. Leoviriyakit and A. Jameson. Aerodynamic shape and planform optimization of wings using a viscous reduced adjoint gradient formula. 2nd M.I.T. Conference on Computational Fluid and Solid Mechanics, Cambridge, MA, June 17-20, 2003.

[17] A. Jameson and S. Shankaran and L. Martinelli. A continuous adjoint method for unstructured grids. 16th AIAA Computational Fluid Dynamics Conference, AIAA Paper AIAA-2003-3955, Orlando, FL, June 23-26, 2003.

[18] J.D. Denton. Loss Mechanisms in Turbomachines. ASME Paper 93-GT-435, 1993.

[19] D.I. Papadimitriou, K.C.Giannakoglou, A Continuous Adjoint Method with Objective Function Derivatives Based on Boundary Integrals for Inviscid and Viscous Flows. Journal of Computers and Fluids, to appear, 2006.

[20] K.C.Giannakoglou, D.I. Papadimitriou. A Continuous Adjoint Method for the Minimization of Losses in Cascade Viscous Flows. AIAA paper 2006-0049, Reno-Nevada, 9-12 January 2006.

[21] D.I. Papadimitriou, K.C.Giannakoglou. Formulation and Application of the Continuous Adjoint Method in Aerodynamics and Turbomachinery. von Karman Institute Lectures Series, 2006.

[22] D.I. Papadimitriou, K.C.Giannakoglou. Compressor Blade Optimization Using a Continuous Adjoint Formulation. ASME TURBO EXPO 2006, GT 2006-90466, 8-11 May 2006, Barcelona, Spain.